Biosensors and Bioelectronics 124–125 (2019) 8–14

Contents lists available at ScienceDirect

Biosensors and Bioelectronics

journal homepage: www.elsevier.com/locate/bios

Design of a simple and novel photoelectrochemical aptasensor for detection of 3,3′,4,4′-tetrachlorobiphenyl

Lifang Fan[a], Caiyun Zhang[a], Huijie Shi[b], Guohua Zhao[b,*]

[a] Institute of Environmental Science, Shanxi University, Taiyuan, Shanxi 030006, China
[b] School of Chemical Science and Engineering, Tongji University, 1239 Siping Road, Shanghai 200092, China

ARTICLE INFO

Keywords:
Aptasensor
3
3′
4
4′-tetrachlorobiphenyl
N-doped TiO_2 nanotubes
Photoelectrochemistry
Polychlorinated biphenyls

ABSTRACT

In view of the urgent need of determining polychlorinated biphenyls in the environment, we developed a highly sensitive and selective photoelectrochemical (PEC) aptasensor for determination of 3,3′,4,4′-tetrachlorobiphenyl (PCB77) by immobilizing aptamer on N-doped TiO_2 nanotubes (N-doped TiO_2 NTs). To improve analytical performance of the PEC sensor, the complementary DNA functionalized CdS quantum dots (DNA-CdS QDs) were introduced onto N-doped TiO_2 NTs by hybridization. In addition of PCB77, owing to high affinity of aptamer to PCB77, PCB77-aptamer complexes were formed by being bound of PCB77 whilst DNA-CdS QDs were released from the sensing surface. The complexes with poor conductivity hindered the interfacial electron transfer, leading to the photocurrent decrease. The more important is the release of DNA-CdS QDs enhanced the photocurrent decrease, playing the role of signal amplification. The photocurrent change was utilized to detect PCB77 quantitatively. The PEC aptasensor exhibited excellent analytical performance for detection of PCB77 with wide linear range of 0.1–100 ng/L and a low detection limit of 0.1 ng/L. It manifested outstanding selectivity for PCB77 in control experiments by employing six interferents which had similar structure or coexisted with PCB77. Besides, the PEC aptasensor was used to detect the content of PBC77 in the environment.

1. Introduction

Polychlorinated biphenyls (PCBs) are a class of ubiquitous, persistent, and highly toxic environmental contaminants, and these compounds have always received widespread attention for the potential risk for human health. Owing to PCBs excellent stability, they are extremely resistant to chemical and biological degradation (Zheng et al., 2016a, 2016b), and often present in surface water, soil and sediment (Sobek and Gustafsson, 2014). Among 209 congeners in PCBs family, PCBs with chlorine in the 3, 4, and 5 positions have similar to the toxic polychlorinated dibenzo-p-dioxins (PCDD) and dibenzofurans (PCDFs) (Johansen et al., 1994). 3,3′,4,4′-tetrachlorobiphenyl (PCB77) is considered to be one of the most toxic dioxin-like PCBs congener that interacts with the aryl hydrocarbon receptor. It not only disturbs the endocrine reproductive system of the organism, but seriously affects the thyroid function, causing biological metabolism disorder, growth abnormalities and stunted growth (Roy et al., 2009). So, it is highly required to develop an effective analytical technique to evaluate the level of PCB77 in the environment.

The common methods for PCBs detection are the instrumental methods, liquid chromatography/mass spectrometry (LC/MS) (Moukas et al., 2014; Lei et al., 2016) and gas chromatography/mass spectrometry (GC/MS) (Muscalu et al., 2015). Although these methods can detect accurately trace PCBs, they involve sophisticated instruments and time-consuming samples preparation procedures. A series of simpler and more effective fluorescent and electrochemical sensors have been developed (Wang and Meng, 2017; Zheng et al., 2016a, 2016b; Wei et al., 2011). But most of them require a complicated procedure for labeling fluorophores or electroactive tags to obtain the detection signal. In recent years, surface enhanced Raman scattering (SERS) sensors with high sensitivity was also reported (Wang et al., 2014). They are very strict with SERS substrate, and only Au or Ag-decorated metal and metal oxide can be qualified for the need. These drawbacks limit actual application of these methods. Most importantly, the individual congener of PCBs is very difficult to be detected quantitatively by the above-mentioned methods because of its extremely low content compared with a majority of PCBs (two or three orders of magnitude) (Malavia et al., 2004). Moreover, in complicated environment, the presence of lots of other organic compounds with high concentration seriously affects the determination of the individual PCBs. Thus, it is still a challenging work to develop a facile, highly sensitive and selective method for detecting the individual PCB77 with low concentration

* Corresponding author.
E-mail address: g.zhao@tongji.edu.cn (G. Zhao).

https://doi.org/10.1016/j.bios.2018.09.054
Received 5 June 2018; Received in revised form 14 September 2018; Accepted 14 September 2018
Available online 15 September 2018
0956-5663/

but high toxicity in the environment.

Photoelectrochemical (PEC) technique as a newly emerged analytical method has attracted more and more research interests (Wang et al., 2017; Qin et al., 2016). The PEC process refers to photon-to-electricity conversion resulting from charge separation and subsequent charge transfer after absorption of photons during illumination (Zhang et al., 2012). In the PEC detection, light is used as the excitation source whilst generated current is used as the detection signal, which is the reverse process to electrochemiluminescence (ECL). (Feng et al., 2015; Yang et al., 2011) Due to the totally separated and two different kinds of energy as excitation source and detection signal resulting in the low background signal, PEC technique is an ultrasensitive analytical method. Furthermore, the application of electronic readout makes the PEC instrument possess these advantages such as favorable portability, fast response, low cost and real-time detection (Zhao et al., 2012; Ren and Liu, 2016). Hence, PEC technique is more favorable to detection of PCB77 at extremely low level of concentration in the environment. However, some active species such as hydroxyl radicals, superoxide anion radicals generated by photoirradiation during PEC detection are such powerful oxidants that most substances will be oxidized on the photoanode (Gong et al., 2012), which makes PEC technique lack of selectivity. How to realize high selectivity while detect sensitively PCB77 in complicated environment is a key problem. Currently , the molecular imprinting (MI) technique has been often used to obtain PEC selective detection of analytes. For instance, our research group developed a cathodic PEC sensor based on Pd quantum dots modified molecularly imprinted TiO_2 nanorods (NRs), and applied in detecting PCB 101 (Shi et al., 2018). However, these MI-based PEC sensors often suffer from these drawbacks such as weak binding sites, slow binding kinetics, and incomplete removal of imprinting molecule from the MIPs surface. The drawbacks limit the actual application of the MI-based PEC sensors. Aptamers are single-strand DNA or RNA sequences with high affinity and specificity for their targets. Aptamer-based analytical techniques are certainly very promising candidates for selective determining analytes. It is reported that the aptamer for highly binding of PCB77 has been selected (Xu et al., 2012). Thus, a PEC sensor based on aptamer as the recognition element is proposed by combining ultrasensitivity of PEC method and high affinity of aptamer for PCB77, and the photocurrent change caused by the biorecognition reaction between aptamer and PCB77 would be utilized for highly sensitive and selective detection of PCB77. Besides, it is very critical to choose an appropriate photoactive material for immobilization of aptamer to get better analytical performance.

At the present, photoactive materials used in PEC biosensor are mainly including inorganic materials such as Si, TiO_2, ZnO and CdS, organic materials such as porphyrin, phthalocyanine and their derivatives, and complex materials. Among these materials, TiO_2 is one of the common photoactive materials for constructing biosensor due to its inexpensiveness, environment safety, chemical and thermal stability. In particular, anodic TiO_2 nanotube arrays (TNs) grown on Ti foil possessing large surface area and high oriented interfacial structure have attracted great interest in the field of PEC sensing.

In this research, the ordered N-doped TiO_2 nanotubes (N-doped TiO_2 NTs) were designed as the photoactive substrate for anchoring aptamer. Owing to their good biocompatibility and highly oriented tubular structure, TiO_2 NTs can provide not only a wonderful microenvironment for aptamer, but also large surface area for loading more aptamer, improving analytical performance of the PEC sensing platform (Chen et al., 2010). By doping N element, the absorption of TiO_2 NTs extends successfully to visible region so that aptamer effectively keep their bioactivity and specificity. Subsequently, the complementary DNA functionalized CdS quantum dots (DNA-CdS QDs) were immobilized on the electrode by hybridization. Here, CdS QDs, as a kind of the popular PEC labels were chosen as DNA-functionalized photoactive material based on their unique electrical and optical properties, and the perfect stability. Thus a facile and novel PEC aptasensor was designed for determining PCB77 in the environment. When PCB77 was added, DNA-CdS QDs were replaced and released from the sensing interface because of high affinity of aptamer to PCB77. The formed aptamer-PCB77 complexes with poor conductivity hindered the electron transfer, resulting in the photocurrent decrease. The release of DNA-CdS QDs further decreased the photocurrent so that the detection signal was amplified. PCB77 could be determined quantitatively by measuring the photocurrent change. The design PEC aptasensor showed high sensitivity and selectivity for detection of PCB77, and the reasons for the excellent analytical performance were explored in detailed. Furthermore, the application of the aptasensor in the environment was also investigated.

2. Experimental

2.1. Reagents and apparatus

The two amino modified oligonucleotides were purchased from Shanghai Sangon Biotechnology Co. Ltd. (Shanghai, China).

aptamer sequence:

5′-GGC-GGG-GCT-ACG-AAG-TAG-TGA-TTT-TTT-CCG-ATG-GCC-CGT-G-$(CH_2)_6$-NH_2–3′

Complementary DNA sequence:

5′-TTC-GTA-GCC-CCG-CCT-TTT-TTT-TTT-TT-$(CH_2)_6$-NH_2–3′

PCB77 and PCB101 were purchased from Beijing Lark Company. Benzopyrene, 17β-estradiol and biphenyl were purchased from Sigma-Aldrich (St. Louis, MO). Titanium foils (≥ 99.8% purity) with the area of 1.5 × 4.0 cm^2 were used in the work. Bovine serum albumin (BSA), N-hydroxy succinimide (NHS), 1-Ethyl-3-(3-dimethylaminopropyl) carbodiimide (EDC), and thioglycolic acid (TGA) were purchased from Aladdin Reagent Co., Ltd. Bisphenol A and atrazine were purchased from Sinopharm Chemical Reagent Co., Ltd. The apparatuses are listed in Supporting information (SI).

2.2. Preparation of N-doped TiO_2 NTs

According to the literature (Antony et al., 2012), Ti foils were mechanically polished prior to anodization. Then cleaned Ti foils were anodized in a two-electrode system with Ti foils as an anode and Pt sheet as a cathode in ethylene glycol solution containing 0.2 wt% carbamide, 0.3 wt% NH_4F and 3 vol% deionized H_2O at 25 °C. The anodization process was performed at 40 V for 3 h. The as-prepared TiO_2 NTs were immersed in ammonium hydroxide for 24 h, followed by annealing in nitrogen ambience at 450 °C for 2 h. The N-doped TiO_2 NTs were used for the following tests. Before use, all of the N-doped TiO_2 NTs were sealed to 1 cm^2 with insulating glue.

2.3. Preparation of water-soluble TGA-CdS QDs and DNA-CdS QDs

TGA-CdS QDs were prepared and the detailed process was supplied in SI. The prepared yellow TGA-CdS QDs were diluted with the same volume of water and stored at 4 °C.

5 mL TGA-CdS QDs, mixed with absolute ethyl alcohol were centrifuged for 3 min. The precipitates, TGA-CdS QDs were dispersed ultrasonically in 5 mL 10 mM PBS (pH 7.41). Then, TGA-CdS QDs were activated by mixing with 20 mg/mL EDC and 10 mg/mL NHS for 30 min. Subsequently, amino-modified DNA (10 μM, 500 μL) was slowly added to the mixture solution and stirred lightly for 12 h. DNA-modified CdS QDs were centrifuged for 30 min at 10,000 rpm to remove the unbound DNA. Finally, DNA-CdS QDs were stored for use at 4 °C.

2.4. Design and fabrication of PEC aptasensor

50 μL 1% chitosan was dropped on N-doped TiO_2 NTs of 1 cm^2 and dried at 40 °C. The electrodes were immersed into 5% (V:V) glutaraldehyde for 30 min. Then 30 μL 3.0 μM aptamer was dropped onto the

electrode surface and stored at 4 °C overnight. Subsequently, the aptamer-modified N-doped TiO_2 NTs was incubated in 30 μL DNA-CdS QDs solution for over 12 h to ensure that DNA-CdS QDs were absolutely hybridized. The prepared aptasensor was immersed 1 wt% BSA to inhibit any unspecific absorption. Finally, it was placed in 0.5% sodium dodecyl sulfate (SDS) solution (pH 1.9) for 3 min and washed with 0.1 M PBS to reuse.

2.5. PEC measurement

All PEC experiments were performed in 0.1 M PBS (pH 7.41) with a 300 W xenon lamp from Perfect Light (Beijing, China) as light source with the wavelength of 430 nm. Photocurrent was recorded by *I-t* technique at the potential of 0.0 V, and the distance was 5 cm between the electrode and the light source. The illumination intensity was 13 mW/cm^2.

In detection of PCB77, photocurrent was investigated when the aptasensor was incubated in different concentrations of PCB77. In control experiments, the aptasensor was used to determine six interferents including PCB101, biphenyl, bisphenol A, benzopyrene, 17β-estradiol and atrazine, and the method was the same as that for detecting PCB77.

3. Results and discussion

3.1. Characterization of PEC aptasensor construction

Scheme 1 illustrates the schematic representation of the PEC aptasensor construction and the detection mechanism for PCB77. The ordered N-doped TiO_2 NTs were first prepared on Ti foils by in situ anodization. After anchoring aptamer on N-doped TiO_2 NTs surface, DNA-CdS QDs were introduced on the sensing interface by hybridizing.

Fig. 1 exhibits the electrochemical impedance spectra (EIS) of each step for the aptasensor construction in the presence of $[Fe(CN)_6]^{3-/4-}$. First, the EIS of N-doped TiO_2 NTs was examined for about 35 kΩ (curve a). After the immobilization of chitosan and glutaraldehyde, NH_2-terminated aptamer molecules were anchored on CHO functionalized electrode surface by the interaction between CHO and NH_2 groups. The EIS value was dramatically increased to 80 kΩ (curve b). This indicated that the negatively charged aptamer molecules were successfully immobilized on N-doped TiO_2 NTs surface, which made an electrostatic repulsion to the negatively charged redox species of $[Fe(CN)_6]^{3-/4-}$. When DNA-CdS QDs were introduced on the electrode by hybridization, the EIS value was again decreased to 58 kΩ (curve c), demonstrating that DNA-CdS QDs could facilitate the electron transfer between the sensing interface and the solution. Finally, after treated with BSA, the obtained aptasensor was incubated in PCB77 solution, and the recognition reaction was guaranteed to complete, a higher EIS value about 90 kΩ was obtained (curve d). This indicated that aptamer-PCB77

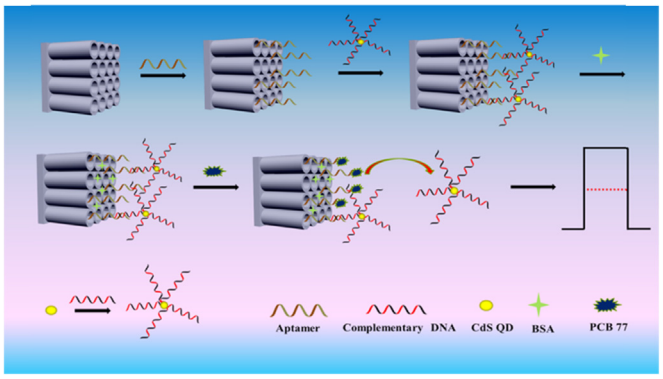

Scheme 1. Schematic representation of PEC aptasensor construction and the detection mechanism of PCB77.

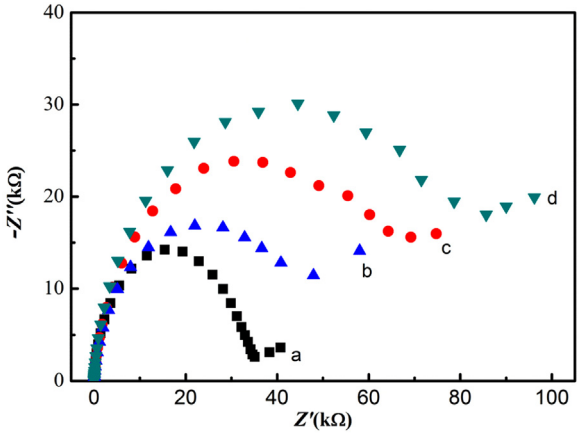

Fig. 1. EIS of (a) N-doped TiO_2 NTs, (b) after aptamer immobilization, (c) after anchoring DNA-CdS QDs, (d) after addition of PCB77.

complexes formed with poorer conductivity than aptamer further hindered the interfacial electron transfer. At the same time, the increasing value of EIS indicated that DNA-CdS QDs may be already released from the sensing interface.

Besides, the PEC characterization of the aptasensor construction was performed and given in Fig. S1. The photocurrent of N-doped TiO_2 NTs was about 12.2 μA cm^{-2}. After modifying aptamer, the photocurrent reduced approximately to 10.79 μA cm^{-2} because of the poor conductivity of aptamer. When the aptamer-modified N-doped TiO_2 NTs was immersed into DNA-CdS QDs solution, the photocurrent was obviously increased to 14.41 μA cm^{-2}, indicating DNA-CdS QDs were successfully immobilized on the sensing interface. Then, the aptasensor was incubated in 0.5 ng/L PCB77 solution after blocking with BSA, the photocurrent remarkably decreased to 12.33 μA cm^{-2}. The PEC characterization results were absolutely consistent with that of EIS characterization, confirming that the PEC aptasensor was successfully constructed.

Here, control experiments were carried out to prove the photocurrent change caused by addition of PCB77. The PEC aptasensor was incubated in the blank solution, 0.1 M PBS, exhibiting high photocurrent and not any photocurrent change. This confirmed that the photocurrent change was attributed to the recognition reaction between aptamer and PCB77. The photocurrent decrement after addition of PCB77 could be explained as follows. Attributing to high affinity of aptamer to PCB77, the binding strength is greater than that between aptamer and its complementary DNA. As a result, PCB77 was captured on N-doped TiO_2 NTs to form the PCB77-aptamer complexes. At the same time, DNA-CdS QDs were replaced and released from the sensing interface. The PCB77-aptamer complexes with poor conductivity increased the hindrances of the interfacial electron transfer, resulting in the decrease of the photocurrent. A more important reason is that the release of the DNA-CdS QDs from the sensing surface make the photocurrent decrease drastically.

3.2. Highly sensitive performance of PEC aptasensor

The photocurrent change was recorded in different concentrations of PCB77 to evaluate the analytical performance of the aptasensor, shown in Fig. 2A. It could be observed that the photocurrent decreased continually with the increase of PCB77 concentrations from 0 to 100 ng/L. This indicated that more and more PCB77-aptamer complexes formed hindered the interfacial electron transfer, and vast DNA-CdS QDs were released from the sensing interface. While PCB77 concentration was over 100 ng/L, the photocurrent was almost no change with increasing PCB77 concentrations from 200 to 500 ng/L. The results demonstrated that DNA-CdS QDs on sensing surface were

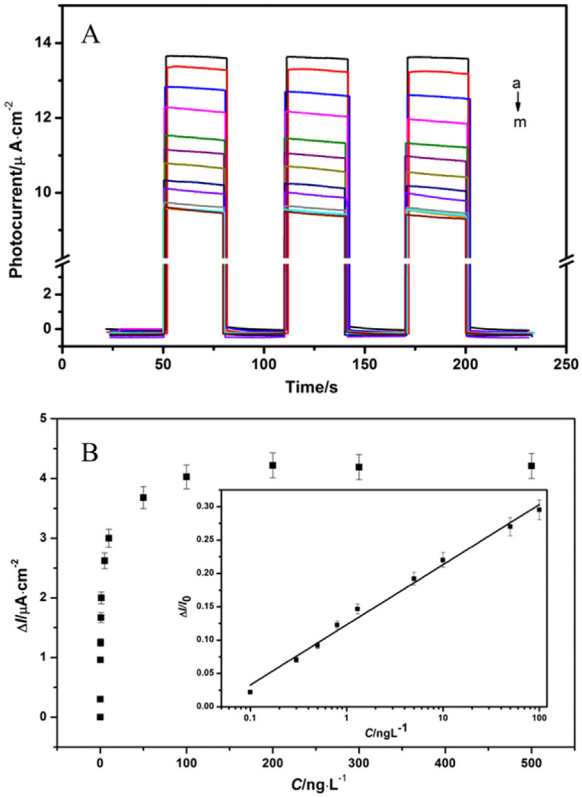

Fig. 2. (A) Photocurrent of the PEC aptasensor to different concentrations of PCB77 from a to m, 0, 0.1, 0.3, 0.5, 0.8, 1.3, 5.0, 10, 50, 100, 200, 300, 500 ng/L, respectively. (B) The relationship of the photocurrent change (ΔI) with different concentrations of PCB77, Inset: the linear calibration curve of ΔI and the logarithm of PCB77 concentrations ranging from 0.1–100 ng/L.

absolutely replaced by PCB77 and the amount of the PCB77-aptamer complexes reached saturation. The curves of the photocurrent change (ΔI) with different concentrations of PCB77 were shown in Fig. 2B, where ΔI was the difference between the photocurrent before (I_0) and after (I) incubation in PCB77. Inset of Fig. 2B showed that the $\Delta I/I_0$ value appeared a well linear relationship with the logarithm of PCB77 concentrations ranging from 0.1 to 100 ng/L. The regression equation was $\Delta I/I_0 = 0.0902 \log C + 0.1229$ (unit of C, ng/L) with a correction coefficient of 0.9900. The detection limit was calculated to be 0.1 ng/L based on the response of three times the standard deviation of zero-pose response (n = 6). So in the practical sample analysis, the concentrations of PCB77 in samples are in the range of 0. 1–100 ng/L, and PCB77 could be accurately determined. Compared with the prior reports, such as the instrument methods (Portolés et al., 2016; Ramanujam et al., 2017), electrochemical sensor (Wei et al., 2011), surface plasmon resonance (Liu et al., 2016) and surface-enhanced Raman scattering techniques (Fu et al., 2015), the detailed comparison results were shown in Table S1. It was found that the detection limit of the present aptasensor for PCB77 detection was lower than that of the conventional instrumental methods and other optical or electrochemical sensors, and the linear working range was comparable or even wider. Such a highly sensitive PEC sensing platform was enough to detect accurately trace PCB77 in the environment. Besides, the two important parameters were investigated before determining PCB77 to obtain the optimum analytical performance. The optimized loading amount of aptamer on N-doped TiO_2 NTs was obtained when the concentration of aptamer was 3 μM. The curve was shown in Fig. S2. To ensure that the biorecognition reaction between aptamer and PCB77 was sufficient, the incubating time of the aptasensor in PCB77 solution was optimized to be 40 min (Fig. S3).

The detailed reasons for the highly sensitive PEC sensing for PCB77 could be exploited from the following aspects.

Firstly, N-doped TiO_2 NTs with the unique tubular structure were design as the appropriate substrate for loading aptamer. Doping nitrogen in TiO_2 NTs was necessary to extend the absorption of TiO_2 to visible region. XPS analysis of the surface composition of N-doped TiO_2 NTs showed nitrogen element present in TiO_2 NTs, and the high resolution spectrum of N-1s was shown in Fig. 3A. The N-1s spectra consisted of three peaks, namely, 399.1, 399.9 and 405.0 eV. The first two peaks were ascribed to substitution nitrogen in the oxide lattice, leading N-Ti-O bond (Romero-Gómez et al., 2009) and the later one was ascribed to surface adsorbed NO_x (Wang et al., 2009). Full-scan XPS spectra of the N-doped TiO_2 NTs and high resolution spectra of other elements were given in Fig. S4. Meanwhile, the UV-DRS spectrum in Fig. 3B showed that the absorption of TiO_2 NTs by doping nitrogen was successfully extended to over 450 nm. This red-shift of the absorption edge was ascribed to the N-doping in the intrinsic band gap of TiO_2 NTs, in the N–Ti–O bond, and the formation of the local state in valence band through the interaction between N2p and O2p orbit could reduce the band gap of TiO_2 NTs, thereby promoting the effective absorption of visible light (Pany and Parida, 2014; Parida et al., 2013). The adsorption of N-doped TiO_2 NTs was in visible region, which was important for maintaining effectively the bioactivity and affinity of aptamer. By measuring the photocurrent under visible irradiation, the results indicated that the photocurrent of N-doped TiO_2 NTs was greatly higher than that of pure TiO_2 NTs (Inset of Fig. 3B). This reason was that a relatively stable oxygen vacancy formed on TiO_2 NTs surface by doping nitrogen enhanced the photoelectric response of TiO_2 NTs (Lai et al., 2010). According to the SEM images shown in Fig. 3C, N-doped TiO_2 NTs of 80–100 nm in diameter were synthesized with the tube wall thickness of approximately 10 nm. Its cross-section view (Inset) showed N-doped TiO_2 NTs was ordered vertically aligned grown on Ti foil with the length of about 2 μm. Compared with pure TiO_2 NTs (Fig. 3D), N-doped TiO_2 NTs surface became slightly rough, which was attributed to the partial lattice collapse of TiO_2 NTs by doping nitrogen. But N-doped TiO_2 NTs still remained intact tubular structure. The high-density and uniform tubes acted as a “nanocontainer”, which not only offered large area nanospaces for immobilizing aptamer, but promoted the directional charge transport due to one-dimensional feature of TiO_2 NTs (Zhang et al., 2013). Besides, the crystal structure of N-doped TiO_2 NTs and TiO_2 NTs was measured by XRD technique (Fig. S5). The diffraction peaks were present at 25.3°, 38.6°, 48.1°, 53.9°, corresponding to (101), (112), (200) and (105) crystal planes, which indicated that N-doped TiO_2 NTs were in anatase phase (JCPDS File 21-1272). The nanocrystal of N-doped TiO_2 NTs was unchanged by doping nitrogen compared with TiO_2 NTs. But the strength of most diffraction peaks weakened, owing to by the disorder of N-doped TiO_2 NTs surface (Li et al., 2009). The Raman spectroscopy analysis in Fig. S6 showed five different Raman vibration peaks were approximately present at 142.1, 192.4, 392.7, 514.4, 636.2 cm^{-1}, corresponding to E_g, E_g, B_{1g}, $A_{1g} + E_g$, E_g mode, which belonged to the modes of anatase phase. The additional absorption mode was not found by doping nitrogen, which was consistent with XRD characterization. So N-doped TiO_2 NTs with tubular structure had better photoelectrical activity, which was conducive to improving the sensitivity of the aptasensor.

Secondly, another important factor for high sensitivity of the PEC aptasensor was that DNA-CdS QDs introduced on the sensing interface enhanced the photocurrent and played the role of signal amplification for detection of PCB77. TEM images in Fig. 4A revealed that TGA-CdS QDs (IR spectra of TAG- CdS QDs was shown in Fig. S7) with the particle size of about 5 nm exhibited excellent dispersion and obvious lattice fringe observed under high resolution TEM from Fig. 4B. The XRD pattern in Fig. 4C showed that the diffraction peaks present at 26.51°, 43.98°, 52.09° could be assigned to (111), (220), and (311) crystal plane (JCPDS, No. 42-1411), demonstrating CdS QDs belonged to the cubic crystal structure, and there was hardly any impure peak. As shown in the inset of Fig. 4C, the UV spectra of TGA-CdS QDs (curve a)

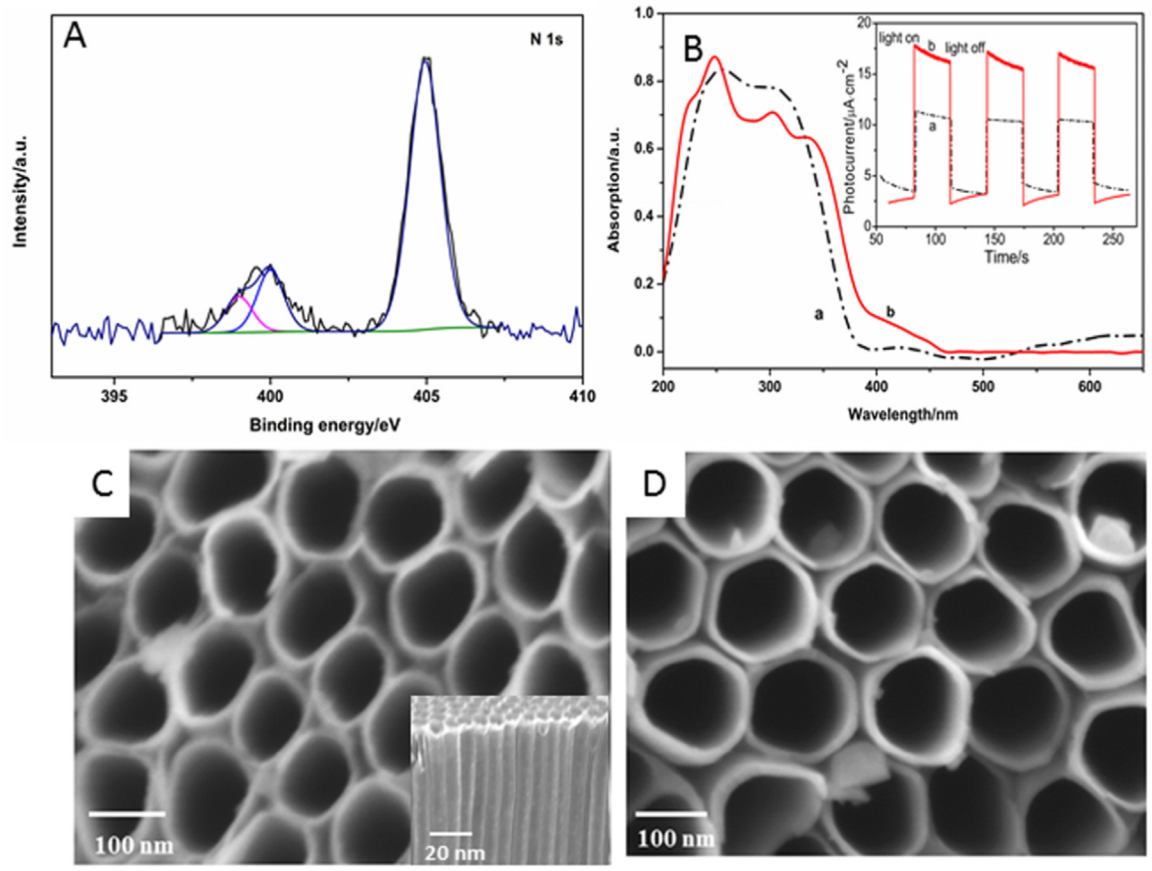

Fig. 3. (A) High resolution XPS spectra of N 1s of N-doped TiO_2 NTs, (B) UV-DRS spectrum of TiO_2 NTs (a) and N-doped TiO_2 NTs (b), Inset: photocurrent of TiO_2 NTs (a) and N-doped TiO_2 NTs (b), (C) SEM top-view images of N-doped TiO_2 NTs and (D) TiO_2 NTs, Inset: the cross-section view of N-doped TiO_2 NTs.

revealed that CdS QDs as an excellent photoactive material exhibited wider light adsorption. A typical characteristic peak of DNA was present at 260 nm for DNA-CdS QDs (curve b), confirming TGA-CdS QDs were successfully labelled with the complementary DNA. TGA-CdS QDs labeled with amino-modified complementary DNA were introduced on the sensing surface, and the SEM morphology and full-scan XPS spectra of the DNA-CdS QDs loaded on N-doped TiO_2 NTs were given in Fig. S8. It was observed that CdS QDs of 5 nm was dispersed on the surface of N-doped TiO2 NTs. The full-scan XPS spectra showed seven elements including S, O, Ti, Cd, N, C and P were present, and the molar ratio of Cd/S was approximately equal to 1.

Here, the photoresponse and the analytical performance of the PEC aptasensor were investigated before and after the introduction of DNA-CdS QDs, shown in Fig. 4D. The photocurrent of the sensor was only about 9.5 μA cm^{-2} without DNA-CdS QDs (curve a), while the photocurrent apparently increased to 13.7 μA cm^{-2} by introducing DNA-CdS QDs on the sensing interface (curve b), demonstrating DNA-CdS QDs helped to enhance the photocurrent of the aptasensor. At the same time, the analytical performance of the PEC aptasensor for detecting 5 ng/L PCB77 was also investigated. The results showed that the photocurrent change, ΔI_b and ΔI_a (the difference of the photocurrent before and after adding PCB77) was 3.1 and 0.30 μA cm^{-2} with (curve b′) and without (curve a′) DNA-CdS QDs, respectively. The photocurrent change of the former was ten times more than the latter. From this, the detection signal was amplified by introducing DNA-CdS QDs. The reason is mainly based on the following mechanism (Freeman et al., 2011; Golub et al., 2009), shown in Fig. S9. Under visible irradiation, CdS QDs absorbed photons with energies higher than its band gap and the electrons were excited from the valence band to the conduction band, forming the electron-hole pairs. The holes participated in oxidation reaction on the electrode surface. The electrons transferred to the electrode and passed through the external circuit, generating photocurrent. Thus more electrons were provided and flowed across the circuit by introducing DNA-CdS QDs, leading to the photocurrent enhancement. In addition of PCB77, owing to high affinity of aptamer to PCB77, the PCB77-aptamer complexes were formed while DNA-CdS QDs were replaced and released from the sensing surface. The PCB77-aptamer complexes with poor conductivity hindered the interfacial electron transfer, resulting in the photocurrent decrease. More importantly, DNA-CdS QDs as a PEC label released from N-doped TiO_2 NTs destroyed the coupling between the photoexcited QDs and the electrode surface. The photogenerated electrons from DNA-CdS QDs decreased dramatically so that the photocurrent of the PEC aptasensor further decreased, and the photocurrent change (detection signal) increased. As a result, DNA-CdS QDs not only increased the photocurrent of the PEC aptasensor, but realized signal amplification for determining PCB77.

Thirdly, the packing density of aptamer molecules on the electrode surface was also a key factor affecting the sensitivity of the PEC aptasensor. The order tubular structure of N-doped TiO_2 NTs with large surface could provide much more multidimensional spaces for loading abundant aptamer, and the packing density of aptamer on N-doped TiO_2 NTs was calculated by the chronocoulometry. The detailed calculation process was supplied in Fig. S10. It was estimated to be 2.36×10^{13} molecules cm^{-2}. Control experiments were performed using gold electrode as the substrate for anchoring aptamer. The packing density of aptamer was approximately 1.24×10^{12} molecules cm^{-2}. The load of aptamer on N-doped TiO_2 NTs was almost twenty times more than that on gold electrode. Besides, compared with our previous work (Fan et al., 2014), the amount of aptamer on N-doped TiO_2 NTs was ten times more than that on CdSe NPs-TiO_2 NTs of 2.26×10^{12} molecules cm^{-2}. It could be understood that a small number of the tubular structure of TiO_2 NTs was inevitable to be

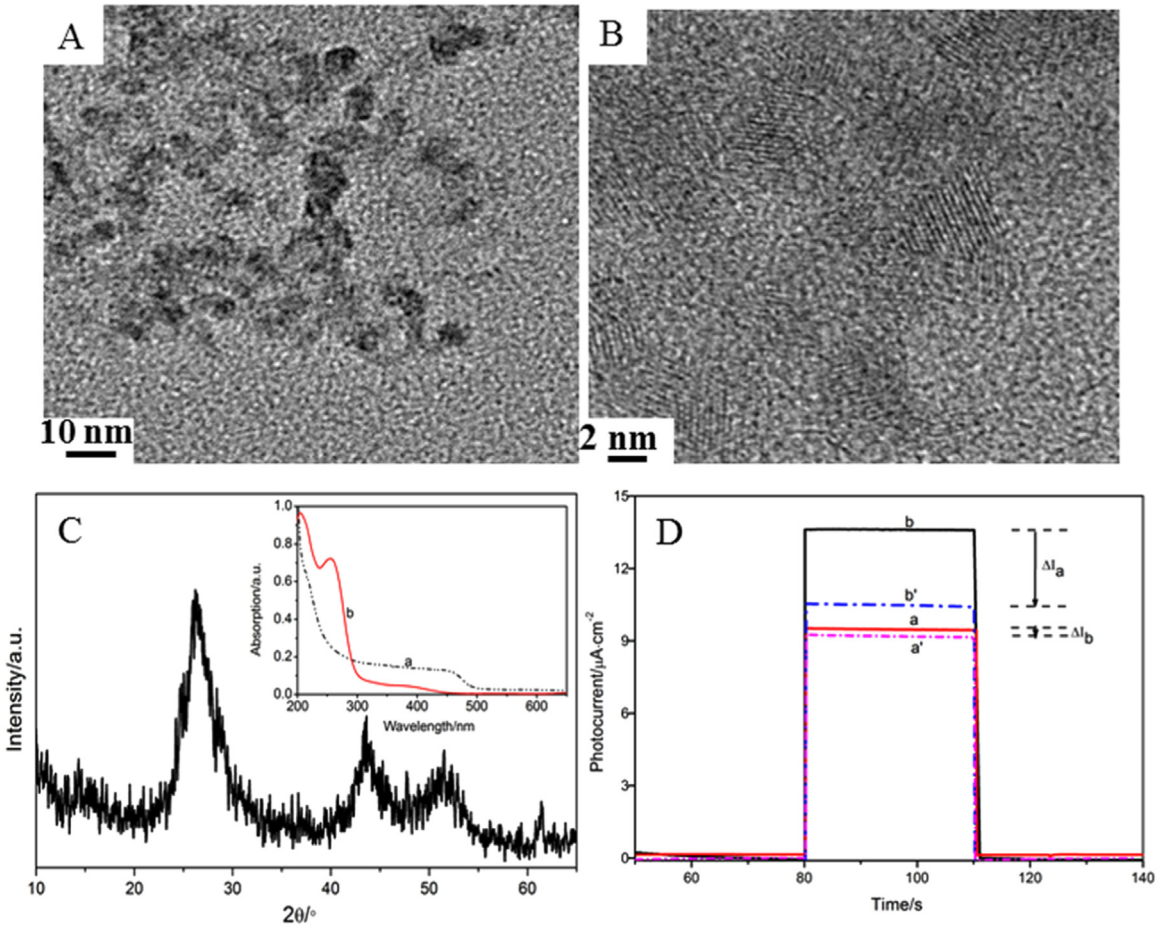

Fig. 4. (A) TEM images and (B) high resolution TEM images of TGA-CdS QDs. (C) XRD patterns of TGA-CdS QDs, Inset: UV spectra of TGA-CdS QDs (a) and DNA-CdS QDs (b). (D) Photoresponse of the PEC sensor before (curve a) and after (curve b) the introduction of DNA-CdS QDs, and their corresponding photocurrent in 0.1 M PBS (pH 7.41) solution containing 5.0 ng/L PCB77 with (curve b′) and without (curve a′) DNA-CdS QDs.

slightly blocked or destroyed when CdSe NPs were electrodeposited on TiO_2 NTs. However, N-doped TiO_2 NTs could keep intact tubular structure of TiO_2 NTs and provided larger nanospaces for immobilizing aptamer molecules. These results further confirmed N-doped TiO_2 NTs were more favorable to load aptamer molecules. The high packing density of aptamer on the sensing interface greatly improved the sensitivity of the aptasensor. Furthermore, due to good biocompatibility and high hydrophilicity of N-doped TiO_2 NTs, aptamer could well retain good bioactivity and high affinity to make per each binding event effectively.

3.3. High selectivity of PEC aptasensor

In order to evaluate the selectivity of the PEC aptasensor for determining PCB77, control experiments were carried out by employing six interferents which might coexist in the environment or have similar structure with PCB77. The aptasensor was incubated in two-component system containing 5 ng/L PCB77 and one interferent with the same concentration. The relative response ($\Delta I_n/\Delta I_0$) of the photocurrent was shown in Fig. 5. $\Delta I_n/\Delta I_0$ was calculated by the photocurrent change ΔI_n (I_n-I_{PCB77}) induced by the interferent in the two-component system versus the photocurrent change ΔI_0 (I_{PCB77}-I_0) for 5 ng/L PCB77, where I_0 and I_{PCB77} referred to the photocurrent before and after incubation in 5.0 ng/L PCB77, I_n was the photocurrent of the two-component system containing 5.0 ng/L PCB77 and another one interferent of the same concentration. It could be observed that $\Delta I_n/\Delta I_0$ was less than 4.57% in the presence of the same concentration of bisphenol A, benzopyrene, 17β-estradiol, atrazine, and less than 7.52% for biphenyl. However,

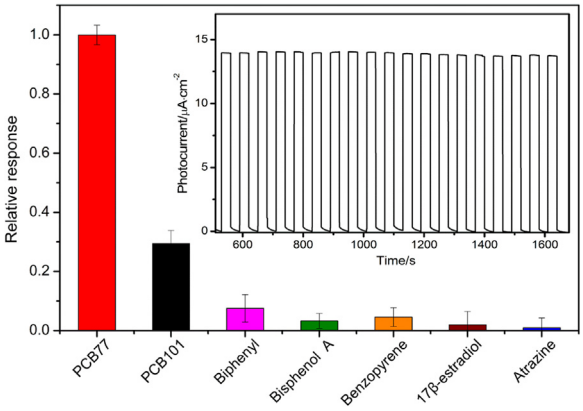

Fig. 5. The selectivity and specificity of the assay for PCB77 on the PEC aptasensor, Inset: Time-based photocurrent response of PEC aptasensor in blank solution.

$\Delta I_n/\Delta I_0$ was 29.4% for PCB101, maybe had an effect on determination of PCB77. Through referring to the original report for selecting anti-PCB77 aptamer by SELEX technique (Xu et al., 2012), we found that the presence of PCB101 interfered similarly on the developed fluorescent aptasensor for the detection of PCB77. The explanation is the fact that the structure of PCB101 was very similar with PCB77. Although the selected aptamer has high affinity and binding ability to PCB77, it could also have a little bit of binding ability with PCB101. So the results obtained in our work are absolutely consistent with that of the original

reference. Thus, other five interferents except for PCB101 couldn't have any interference on the PEC aptasensor for the detection of PCB77.

3.4. Stability, reproducibility and reusability of PEC aptasensor

The stability of the aptasensor was very critical factor in practical application. Its photocurrent was investigated as the excitation light was turned on and off repeatedly, shown in the inset of Fig. 5. It was observed that the photocurrent hadn't any change over 20 min, revealing the perfect stability of the PEC aptasensor. Besides, its long-term storage was also studied when stored in 0.1 M PBS (pH 7.41) at 4 °C for two weeks. The photocurrent still remained 93.2% of the initial response for detecting the same concentration of PCB77, demonstrating good long-term stability of the PEC aptasensor. The stability could be related with the immobilization way of aptamer on the photoactive material and the special 3-D nanotubular structure of N-doped TiO_2 NTs (Yu et al., 2010).

The reproducibility of the PEC aptasensor was evaluated by an intraassay and an interassay. The intraassay was for determining 0.5 ng/L PCB77 with six replicate measurements and the relative standard deviation (RSD) was 6.12%. The interassay RSD was 6.25% by detecting 0.5 ng/L PCB77 with five aptasensors. The results suggested that the PEC aptasensor had good reproducibility, which was suitable to be applied to detecting the actual samples. Besides, the reusability of the aptasensor was also investigated. The PCB77-aptamer complexes on the electrode could be effectively eliminated in 0.5% SDS solution (pH 1.9) for 3 min. The photocurrent response after regeneration was shown in Fig. S11. Over 80% of the initial response was observed after reuse for three times.

3.5. Practical application of PEC aptasensor

The PEC aptasensors were used to determine the real samples, tap water and domestic sewage using the standard addition method. Before analysis, the sewage samples were filtered through an ordinary filter paper to remove the suspended solid matter and small particles and then they were further pretreated by the membrane with the size of 0.2 μm. The substances dissolved in these samples were not changed by the pretreatment. The samples were diluted to decrease the interference of complex matrices. These samples spiked with three different concentrations of 5, 15 and 60 ng/L were detected, respectively. The recovery results of PCB77 in the two different matrixes were showed in Table S2. In order to demonstrate accuracy and reliability of the PEC aptasensor, HPLC was used to analyze the same samples. Seen from Table S2, the results with the present aptasensor are well consistent with that obtained by HPLC. The RSD of the two methods are less than 6.0% based on five experiments at each concentration. It confirmed the practicality of the present aptasensor for the detection of PCB 77. More importantly, compared with HPLC, the present method is simpler, rapider and more low-cost without complex sample preparation, specialized personnel operation and expensive instruments. Meanwhile, the results indicated that the PEC aptasensor could resist the influence of complex matrix effect, and exhibited good accuracy and high precision.

4. Conclusions

In summary, a simple and novel PEC aptasensor was constructed for detection of PCB77 by immobilizing aptamer on N-doped TiO_2 NTs. Through introducing DNA-CdS QDs on the sensing interface, it enhanced the photocurrent and amplified the detection signal for PCB77, improving effectively the sensitivity of the aptasensor. The PEC aptasensor exhibited good sensitivity, selectivity and stability. Meanwhile, it was successfully applied to evaluate PBC77 levels in real samples, and the results were acceptable.

Acknowledgements

This work was financially supported by the National Natural Science Foundation of China (NSFC, No. 21707082, 21537003 and 21677110), and the Natural Science Foundation of Shanxi Province (201601D102008).

Appendix A. Supporting information

Supplementary data associated with this article can be found in the online version at doi:10.1016/j.bios.2018.09.054.

References

Antony, R.P., Mathews, T., Panda, K., Sundaravel, B., Dash, S., Tyagi, A.K., 2012. J. Phys. Chem. C 116, 16740–16746.
Chen, D., Zhang, H., Li, X., Li, J.H., 2010. Anal. Chem. 82, 2253–2261.
Fan, L.F., Zhao, G.H., Shi, H.J., Liu, M.C., Wang, Y.B., Ke, H.Y., 2014. Environ. Sci. Technol. 48, 5754–5761.
Feng, X.B., Gan, N., Zhang, H.R., Yan, Q., Li, T.H., Cao, Y.T., Hu, F.T., Yu, H.W., Jiang, Q.L., 2015. Biosens. Bioelectron. 74, 587–593.
Freeman, R., Willner, B., Willner, I., 2011. J. Phys. Chem. Lett. 2, 2667–2677.
Fu, C.C., Wang, Y., Chen, G., Yang, L.Y., Xu, S.P., Xu, W.Q., 2015. Anal. Chem. 87, 9555–9558.
Golub, E., Pelossof, G., Freeman, R., Zhang, H., Willner, I., 2009. Anal. Chem. 81, 9291–9298.
Gong, J.M., Wang, X.Q., Li, X., Wang, K.W., 2012. Biosens. Bioelectron. 38, 43–49.
Johansen, H.R., Becher, G., Greibrokk, T., 1994. Anal. Chem. 66, 4068–4073.
Lai, Y.K., Huang, J.Y., Zhang, H.F., Subramaniam, V.P., Tang, Y.X., Gong, D.G., Sundar, L., Sun, L., Chen, Z., Lin, C.J., 2010. J. Hazard. Mater. 184, 855–863.
Lei, Y., He, M., Chen, B.B., Hu, B., 2016. Talanta 150, 310–318.
Li, G.S., Yu, J.C., Zhang, D.Q., Hu, X.L., Lau, W.M., 2009. Sep. Purif. Technol. 67, 152–157.
Liu, J., Cai, H., Chen, C., Yang, G., Yang, C.F., 2016. Sensors 16, 1241–1256.
Malavia, J., Santos, F.J., Galceran, M.T., 2004. J. Chromatogr. A 1056, 171–178.
Moukas, A.I., Thomaidis, N.S., Calokerinos, A.C., 2014. J. Mass Spectrom. 49, 1096–1107.
Muscalu, A.M., Edwards, M., Gorecki, T., Reiner, E.J., 2015. J. Chromatogr. A 1391, 93–101.
Pany, S., Parida, K.M., 2014. ACS Sustain. Chem. Eng. 2, 1429–1438.
Parida, K.M., Pany, S., Naik, B., 2013. J. Hydrog. Energ. 38, 3545–3553.
Portolés, T., Sales, C., Abalos, M., Sauló, J., Abad, E., 2016. Anal. Chim. Acta 937, 96–105.
Qin, Xj, Xu, S.X., Deng, L., Huang, R.F., Zhang, X.F., 2016. Biosens. Bioelectron. 85, 957–963.
Ramanujam, N., Sivaselvakumar, M., Ramalingam, S., 2017. Biomed. Chromatogr. 31, 1–6.
Ren, S.T., Liu, W.J., 2016. J. Mater. Chem. A 4, 2236–2245.
Romero-Gómez, P., Rico, V., Borrás, A., Barranco, A., Espinós, J.P., Cotrino, J., González-Elipe, A.R., 2009. J. Phys. Chem. C 113, 13341–13351.
Roy, T.A., Hammerstrom, K., Schaum, J., 2009. J. Toxicol. Environ. Health Part A 72, 350–357.
Shi, H.J., Wang, Y.L., Zhao, J.Z., Huang, X.R., Zhao, G.H., 2018. J. Hazard. Mater. 342, 131–138.
Sobek, A., Gustafsson, O., 2014. Environ. Sci. Technol. 48, 6719–6725.
Wang, J., Tafen, D.N., Lewis, J.P., Hong, Z., Manivannan, A., Zhi, M., Li, M., Wu, N., 2009. J. Am. Chem. Soc. 131, 12290–12297.
Wang, M.L., Meng, G.W., 2017. Sens. Actuators B 243, 1137–1147.
Wang, X.P., Xu, R., Sun, X., Wang, Y.G., Ren, X., Du, B., Wu, D., Wei, Q., 2017. Biosens. Bioelectron. 96, 239–245.
Wang, Z.W., Meng, G.W., Huang, Z.L., Li, Z.B., Zhou, Q.T., 2014. Nanoscale 6, 15280–15285.
Wei, Y., Kong, L.T., Yang, R., Wang, L., Liu, J.H., Huang, X.J., 2011. Chem. Commun. 47, 5340–5342.
Xu, S.M., Yuan, H., Chen, S.P., Xu, A., Wang, J., Wu, L.J., 2012. Anal. Biochem. 423, 195–201.
Yang, L.Z., Jing, Z., Xu, Y., Yun, W., Zhang, R.Y., He, P.G., Fang, Y.Z., 2011. Electroanalysis 23, 1007–1012.
Yu, Z.M., Zhao, G.H., Liu, M.C., Lei, Y.Z., Li, M.F., 2010. Environ. Sci. Technol. 44, 7878–7883.
Zhang, L., Mohamed, H.H., Dillert, R., Bahnemann, D., 2012. J. Photochem. Photobiol C: Photochem. Rev. C13, 263–276.
Zhang, Y.Y., Cao, T.C., Huang, X.F., Liu, M.C., Shi, H.J., Zhao, G.H., 2013. Electroanalysis 25, 1787–1795.
Zhao, W.W., Ma, Z.Y., Yan, D.Y., Xu, J.J., Chen, H.Y., 2012. Anal. Chem. 84, 10518–10521.
Zheng, J., Yu, L.H., Chen, S.J., Hu, G.C., Chen, K.H., Yan, X., Luo, X.J., Zhang, S., Yu, Y.J., Yang, Z.Y., Mai, B.X., 2016a. Environ. Sci. Technol. 50, 1579–1586.
Zheng, X.L., Li, H.L., Xia, F.Q., Tian, D., Hua, X.X., Qiao, X.Y., Zhou, C.L., 2016b. Electrochim. Acta 194, 413–421.